PTEP

Prog. Theor. Exp. Phys. **2021**, 043A01 (21 pages)
DOI: 10.1093/ptep/ptab034

Symmetry enhancement in a two-logarithm matrix model and the canonical tensor model

Naoki Sasakura*

Yukawa Institute for Theoretical Physics, Kyoto University, Kitashirakawa, Sakyo-ku, Kyoto 606-8502, Japan
*E-mail: sasakura@yukawa.kyoto-u.ac.jp

Received August 25, 2020; Revised February 4, 2021; Accepted March 5, 2021; Published March 12, 2021

We study a one-matrix model of a real symmetric matrix with a potential which is a sum of two logarithmic functions and a harmonic one. This two-logarithm matrix model is the absolute square norm of a toy wave function which is obtained by replacing the tensor argument of the wave function of the canonical tensor model (CTM) with a matrix. We discuss a symmetry enhancement phenomenon in this matrix model and show that symmetries and dimensions of emergent spaces are stable only in a phase which exists exclusively for the positive cosmological constant case in the sense of CTM. This would imply the importance of the positivity of the cosmological constant in the emergence phenomena in CTM.

Subject Index A13, B83, E05

1. Introduction

Quantum gravity is one of the serious fundamental problems in theoretical physics. The problem originates from the fact that it is difficult to apply the standard quantum field theoretical method to the quantization of general relativity.[1] Various approaches have been proposed, and some of them argue that macroscopic spacetimes and general relativity are emergent phenomena from collective dynamics of some fundamental degrees of freedom [2–5].

The tensor model may be regarded as one such approach [6–9]. It was introduced as an extension of the matrix model, which successfully describes two-dimensional quantum gravity [10], with the hope of extending the success to higher dimensions. However, the tensor model does not seem to generate macroscopic spacetimes but is rather dominated by singular objects like branched polymers.[2] Therefore, it seems difficult to regard the tensor model as quantum gravity for dimensions higher than two.

The tensor model above is considered in the context of Euclidean simplicial quantum gravity. In fact, simplicial quantum gravity is more successful in the Lorentzian context. It has been shown that causal dynamical triangulation, the Lorentzian version, successfully generates macroscopic spacetimes [13], while dynamical triangulation, the Euclidean version, does not. Prompted by the success, the present author has formulated a tensor model in the Hamilton formalism, which we call the canonical tensor model (CTM) [14,15]. CTM is a first-class constrained system having an analogous structure to the Arnowitt–Deser–Misner formalism of general relativity. The canonical

[1] However, see, for example, Ref. [1] for a sophisticated quantum field theoretical approach.
[2] See Refs. [11,12] for a proof in the large-N limit in the colored tensor model.

Funded by SCOAP[3]

quantization of CTM is straightforward [16], and the physical state condition can be solved exactly by a wave function [17].

The wave function is represented by a multiple integral of an integrand which has an argument of a real symmetric tensor P_{abc} $(a, b, c = 1, \ldots, N)$ [17] (see Appendix A for a minimal introduction). It has been argued in general contexts and has been shown for some simple cases that the wave function has peaks at Lie group symmetric configurations (namely, $P_{abc} = g^{a'}_a g^{b'}_b g^{b'}_b P_{a'b'c'}, g \in G$) for various Lie group representations G [18,19]. This phenomenon, which may be called symmetry emergence from quantum coherence, would be interesting from the perspective of spacetime emergence, since spacetimes could potentially be realized as gauge orbits of Lie group representations.[3] However, we need more thorough knowledge of the phenomenon to argue for spacetime emergence, including the large-N limits, in which continuum spacetimes are expected to appear.

In Refs. [20–23] we studied the wave function in the negative cosmological constant case through a matrix model with non-pairwise index contractions. However, real interesting properties of CTM are expected to appear in the positive cosmological constant case, since the symmetry emergence phenomenon mentioned above is much more evident in the positive case than the negative [19]. Here, the Monte Carlo simulations performed in Refs. [21–23] cannot easily be applied, because the quantity to be computed for the positive case suffers from the notorious sign problem of Monte Carlo simulations.

In this paper we consider a matrix version of the wave function of CTM by replacing the tensor argument P_{abc} with a matrix M_{ab}. This of course is not an approximation to the wave function, but its similarity makes the correspondence of the parameters and the interpretations between the matrix and the tensor versions possible. An advantage of the matrix version is that it can be computed even for the positive cosmological constant case, as we will see. As will be explained in Sect. 2, the matrix model we consider comes from the absolute square norm of the matrix version of the wave function, and is given by a one-matrix model of a real symmetric matrix M_{ab} $(a, b = 1, 2, \ldots, N)$ with a partition function defined by

$$Z = \int_{\mathbb{R}^{\#M}} \prod_{\substack{a,b=1 \\ a \le b}}^{N} dM_{ab}\, e^{-S(M)}, \tag{1}$$

where $\#M = N(N+1)/2$ (the number of independent components of M_{ab}), and

$$S(M) := \mathrm{Tr}\left[\frac{R}{2}\log(k_1 + ik_2 - iM) + \frac{R}{2}\log(k_1 - ik_2 + iM) + \alpha M^2\right], \tag{2}$$

with positive parameters R, k_1, k_2, and α. The parameters have a redundancy under the rescaling of M_{ab}, and $\alpha = 1$ may be taken in the following sections.

A similar matrix model with two logarithmic functions has been considered in a different context in Ref. [24] with a difference in the last term of Eq. (2).

2. Connection to the canonical tensor model

As explained in Appendix A, Eq. (A.4) gives the wave function corresponding to the exactly solved physical state [17] of CTM mentioned in Sect. 1. We consider an analogous wave function which is

[3] In fact, the peaks of the wave function of CTM form ridges along configurations invariant under Lorentzian Lie groups, such as $SO(n, 1)$, rather than Euclidean Lie groups [19].

obtained by replacing P_{abc} with M_{ab}:

$$\Psi(M) := \langle M|\Psi\rangle = \varphi(M)^R,$$
$$\varphi(M) := \int_{\mathbb{R}^N} \prod_{a=1}^{N} d\phi_a \, e^{iM_{ab}\phi_a\phi_b - (k_1+ik_2)\phi_a\phi_a}, \tag{3}$$

where the repeated indices are assumed to be summed over. Here, the integration region is the whole N-dimensional real space, M_{ab} is a real symmetric matrix, and k_1, k_2, and R are assumed to be positive.[4] The part containing k_1 and k_2 of the integrand is an analogue to the Airy function in Eq. (A.4). If k_1 dominates, the part becomes a damping function corresponding to the negative cosmological constant case in CTM, while, if k_2 dominates, the part becomes oscillatory corresponding to the positive cosmological constant case. As explained in Sect. 1, since we are mainly interested in the positive cosmological constant case, our main focus is on the case with finite k_2 and small k_1. More precisely, $\tilde{k}_1 = k_1/\sqrt{N} \ll 1$ (which will appear later) is implicitly assumed throughout this paper.

Let us consider the following observable for the state $|\Psi\rangle$ in Eq. (3):

$$\langle\Psi|e^{-\alpha\hat{M}^2}|\Psi\rangle = \int_{\mathbb{R}^{\#M}} \prod_{\substack{a,b=1\\ a\le b}}^{N} dM_{ab} \, |\Psi(M)|^2 \, e^{-\alpha M^2}, \tag{4}$$

where α is a positive parameter, $M^2 := M_{ab}M_{ab}$, and the integration is over the whole $\#M$-dimensional real space. By performing the Gaussian integration over ϕ_a in Eq. (3) and putting the result into Eq. (4), we obtain

$$\langle\Psi|e^{-\alpha\hat{M}^2}|\Psi\rangle = \text{const.}\, Z, \tag{5}$$

where Z is given in Eq. (1), and the overall constant is irrelevant.

It would be instructive to cast the same system into a different expression. Let us assume R is an integer. Then the Rth power of the wave function in Eq. (3) can be replaced by introducing R replicas of ϕ_a:

$$\Psi(M) = \varphi(M)^R = \int_{\mathbb{R}^{NR}} \prod_{a,l=1}^{N,R} d\phi_a^l \, e^{\sum_{l=1}^{R} iM_{ab}\phi_a^l\phi_b^l - (k_1+ik_2)\phi_a^l\phi_a^l}. \tag{6}$$

Considering the same replacement for the complex conjugate $\Psi^*(M)$ with variable $\tilde{\phi}_a^l$, putting them into Eq. (4), and integrating over M, we obtain

$$Z = \text{const.} \int \prod_{a,l=1}^{N,R} d\phi_a^l d\tilde{\phi}_a^l \, e^{-S_\phi}, \tag{7}$$

where

$$S_\phi := \frac{1}{4\alpha}\left(\mathrm{Tr}\left[\phi\phi^t\phi\phi^t\right] + \mathrm{Tr}\left[\tilde{\phi}\tilde{\phi}^t\tilde{\phi}\tilde{\phi}^t\right] - 2\mathrm{Tr}\left[\phi\phi^t\tilde{\phi}\tilde{\phi}^t\right]\right)$$
$$+ (k_1+ik_2)\mathrm{Tr}\left[\phi\phi^t\right] + (k_1-ik_2)\mathrm{Tr}\left[\tilde{\phi}\tilde{\phi}^t\right], \tag{8}$$

[4] The sign of k_2 can always be chosen positive by the replacement $M \to -M$ without loss of generality for our discussions in later sections (see Eq. (13), for example).

where $(\phi\phi^t)_{ab} := \sum_{l=1}^{R} \phi_a^l \phi_b^l$. This may be regarded as a special choice of the parameters of the eight-vertex matrix model presented in Ref. [25]. It can also be regarded as a usual matrix analogue to the matrix model with non-pairwise index contractions analyzed in Refs. [20–23] in the context of CTM.

Though there would be no direct quantitative connections between the matrix and tensor models, the problem we consider in the matrix model and that of the tensor model have a certain common characterization, as described below. For simplicity, let us put $k_1 = 0$, which is consistent with our purpose as explained above. Then, the "matrix model wave function" $\varphi(M)$ in Eq. (3) has peaks of infinite values at the locations where k_2 is an eigenvalue of M, because $\varphi(M) \propto \det(M_{ab} - k_2\delta_{ab})^{-\frac{1}{2}}$. In other words,[5] the matrix model in Eq. (5) has a preference for configurations of M such that the curve $S(M,\phi) = 0$ in the space of ϕ_a, where $S(M,\phi)$ is the exponent of the integrand in Eq. (3), has singular points in ϕ_a defined by

$$\frac{\partial}{\partial \phi_a} S(M,\phi) = 2M_{ab}\phi_b - 2k_2\phi_a = 0, \tag{9}$$

which is the condition for an eigenvalue of M to be k_2. The full dynamics of the matrix model is determined by the balance between this preference for the curve $S(M,\phi) = 0$ to be singular and the repulsive nature of eigenvalues of random matrices.

This characterization of the problem also holds for the tensor model. As discussed in Sect. 4.2 of Ref. [19], the peaks (singular points) of the wave function in Eq. (A.3) are located where the curve $S_{\mathrm{CTM}}(P,\phi,\tilde{\phi}) = 0$ in the space of $\phi_a, \tilde{\phi}$, where $S_{\mathrm{CTM}}(P,\phi,\tilde{\phi})$ is the exponent of the integrand in Eq. (A.3), has singular points in $\phi_a, \tilde{\phi}$ defined by

$$\frac{\partial}{\partial \phi_a} S_{\mathrm{CTM}}(P,\phi,\tilde{\phi}) = \frac{\partial}{\partial \tilde{\phi}} S_{\mathrm{CTM}}(P,\phi,\tilde{\phi}) = 0. \tag{10}$$

Therefore, there are similar preferences for the curve $S_{\mathrm{CTM}}(P,\phi,\tilde{\phi}) = 0$ to be singular as in the matrix model. However, the dynamics among eigenvalues/vectors would be more complicated than the matrix model due to the non-linear (namely, third-order) character of $S_{\mathrm{CTM}}(P,\phi,\tilde{\phi})$ in $\phi_a, \tilde{\phi}$.

3. Aligned Coulomb gas picture

In this section we give an intuitive picture of the dynamics of the matrix model in Eq. (1) by regarding it as an aligned Coulomb gas system. A solid treatment of the matrix model by the Schwinger–Dyson equation will be discussed in Sect. 4.

The partition function of the matrix model can be rewritten by using its invariance under the $SO(N)$ transformation $M' = LML^t$, $L \in SO(N)$. Denoting the eigenvalues of M by λ_a $(a = 1, 2, \ldots, N)$, which are all real, one obtains

$$Z = \text{const.} \int_{\mathbb{R}^N} \prod_{a=1}^{N} d\lambda_a \prod_{\substack{a,b=1 \\ a<b}}^{N} |\lambda_a - \lambda_b| \, e^{-\sum_{a=1}^{N} S(\lambda_a)} \tag{11}$$

$$= \text{const.} \int_{\mathbb{R}^N} \prod_{a=1}^{N} d\lambda_a \, e^{-S_{\mathrm{Coul}}(\lambda)}, \tag{12}$$

[5] For instance, see Ref. [29] for the view to regard the eigenvalue/vector problem for matrices and tensors as discriminants for curves.

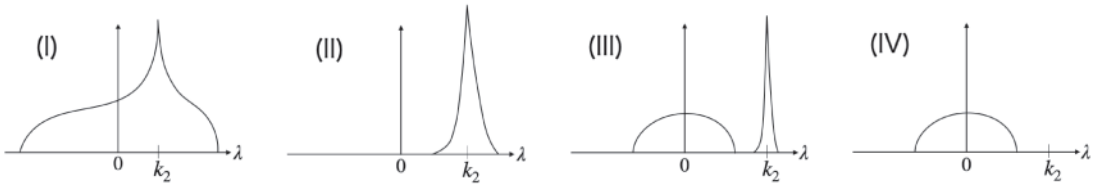

Fig. 1. The four possible profiles of the eigenvalue distributions for the matrix model in Eq. (1).

where $\prod_{a<b}|\lambda_a - \lambda_b|$ is the Jacobian for the change of variable from M to λ_a (and integrate over L), and

$$S_{\rm Coul}(\lambda) := -\sum_{\substack{a,b=1\\a<b}}^{N} \log|\lambda_a - \lambda_b| + R\sum_{a=1}^{N}\log|\lambda_a - k_2 + ik_1| + \alpha\sum_{a=1}^{N}\lambda_a^2. \tag{13}$$

The form of $S_{\rm Coul}(\lambda)$ in Eq. (13) shows that the eigenvalue system can be interpreted as a system of charged particles on a line interacting with each other by the two-dimensional Coulomb potentials. More precisely, the first term represents that the particles of unit charge are located at λ_a ($a = 1, 2, \ldots, N$) on $\mathbb{R}$ and interact with each other by the Coulomb repulsive potentials. The second term can be interpreted as that there exists an opposite charge $-R$ located at a fixed location k_2 interacting with the particles of unit charge by its Coulomb potential. Here, k_1 can be regarded as a sort of small regularization parameter to the potential, since, as explained in Sect. 2, our main interest is the case of small k_1 corresponding to the positive cosmological constant case in CTM. The third term represents a harmonic potential for all the particles.

While the first and the third terms generate the eigenvalue distribution of the semicircle law [26], the second term generated by the $-R$ charge attracts the particles to the neighborhood of k_2, and part of the $-R$ charge is screened. Therefore, we can expect the following four possibilities of eigenvalue distributions to occur, as shown in Fig. 1:

(I) For small R and small k_2, there is a semicircle-like distribution with a concentration (peak) around k_2.
(II) For large R, all the eigenvalues concentrate around k_2.
(III) For large R and large k_2, there are two bunches of eigenvalues, one with a semicircle-like distribution and the other around k_2.
(IV) For small R and large k_2, the eigenvalues form a semicircle-like distribution with no concentration around k_2.

Here, note that all the parameters R, k_1, k_2, and α are assumed to be positive, as mentioned below Eq. (2).

Next, let us discuss the large-N limit in a manner similar to Ref. [27]. To balance all the terms in Eq. (13), the scaling with N can be determined to be

$$\begin{aligned} R &= N\tilde{R},\\ k_i &= \sqrt{N}\tilde{k}_i,\\ \lambda_a &= \sqrt{N}\tilde{\lambda}_a, \end{aligned} \tag{14}$$

where $\tilde{R}$, $\tilde{k}_i$, and $\tilde{\lambda}_a$ are supposed to be kept finite in the limit. By introducing a distribution function $\rho(\tilde{\lambda})$ for the eigenvalues, the $S_{\rm Coul}$ in Eq. (13) can be rewritten in the large-N limit as

$$S_{\rm cont}(\rho) = N^2\left[-\frac{1}{2}\int_{\mathbb{R}^2} dxdy\,\rho(x)\rho(y)\log|x-y| + \int_{\mathbb{R}} dx\,\rho(x)\left(\tilde{R}\log|x-\tilde{k}_2+i\tilde{k}_1| + \alpha x^2\right)\right], \tag{15}$$

where we have ignored an additional irrelevant constant, and have taken the normalization of ρ as

$$\int_{\mathbb{R}} dx\,\rho(x) = 1 \tag{16}$$

for $\sum_{a=1}^{N}\cdots \to N\int_{\mathbb{R}} dx\,\rho(x)\cdots$.

After adding the Lagrange multiplier $\beta(\int dx\rho(x)-1)$ to take into account the constraint in Eq. (16), the functional derivative of $S_{\rm cont}$ with respect to $\rho(x)$ leads to the stationary equation

$$-\int_{\mathbb{R}} dy\,\rho(y)\log|x-y| + \tilde{R}\log|x-\tilde{k}_2+i\tilde{k}_1| + \alpha x^2 + \beta = 0. \tag{17}$$

Note that this is valid only in the region of x with $\rho(x) > 0$, because there is a physical constraint $\rho(x) \geq 0$ and the functional derivative cannot freely be taken in the region $\rho(x) = 0$. Taking further the derivative of Eq. (17) with respect to x, we have

$$-\!\!\!\!\!\!\int_{\mathbb{R}} dy\frac{1}{x-y}\rho(y) = \frac{\tilde{R}(x-\tilde{k}_2)}{(x-\tilde{k}_2)^2+\tilde{k}_1^2} + 2\alpha x, \tag{18}$$

where the integration with a dash represents the Cauchy principal value. This equation will be treated by using the Schwinger–Dyson equation of the matrix model in the large-N limit in Sect. 4.

4. Analysis by the Schwinger–Dyson equation

In this section we will study the matrix model in Eq. (1) in the large-N limit by the Schwinger–Dyson equation. See, for example, Ref. [10] for some details of the techniques used in this section.

Let us define

$$W(z) := \frac{1}{N}\left\langle \mathrm{Tr}\left[\frac{1}{z-M}\right]\right\rangle, \tag{19}$$

where z is a complex variable, and $\langle\cdot\rangle$ denotes the expectation value in the matrix model. Since we consider real symmetric M, the singularities of $W(z)$ can only be on the real axis. As we will see below, $W(z)$ has branch cuts of square roots on the real axis, and the eigenvalue density $\rho(x)$ on real x is related to $W(z)$ by

$$\rho(x) = \frac{i}{2\pi}\left[W(x+i\,\epsilon) - W(x-i\,\epsilon)\right] \tag{20}$$

with $\epsilon = +0$.

Let us consider the Schwinger–Dyson equation,

$$\int_{\mathbb{R}^{\#M}} \prod_{\substack{a,b=1\\ a\leq b}}^{N} dM_{ab}\, D^M_{cd}\left\{\left(\frac{1}{z-M}\right)_{cd} e^{-S(M)}\right\} = 0, \tag{21}$$

where D^M_{ab} denotes the partial derivative with respect to M_{ab} defined by

$$D^M_{ab} M_{cd} = \delta_{ac}\delta_{bd} + \delta_{bc}\delta_{ad}, \tag{22}$$

with the symmetric property of the indices of M_{ab} being taken into account. By taking derivatives on the left-hand side of Eq. (21), we obtain

$$\int \prod_{\substack{a,b=1\\ a\le b}}^{N} dM_{ab} \left\{ \left(\frac{1}{z-M}\right)_{cc} \left(\frac{1}{z-M}\right)_{dd} + \left(\frac{1}{z-M}\right)_{cd} \left(\frac{1}{z-M}\right)_{dc} - 2\left(\frac{1}{z-M}\right)_{cd} S'(M)_{dc} \right\} e^{-S(M)} = 0. \tag{23}$$

Let us perform the large-N limit given in Eq. (14), where the last one corresponds to $M \to \sqrt{N}M$ (accompanied by $z \to \sqrt{N}z$). Then, in the leading order of N, by assuming the factorization for the first term and ignoring the second term as sub-leading, we obtain

$$W(z)^2 - \frac{2}{N}\left\langle \mathrm{Tr}\left[\frac{\tilde{S}'(M)}{z-M}\right]\right\rangle = 0, \tag{24}$$

where

$$\tilde{S}'(M) = \frac{\tilde{R}}{2(M-\tilde{k}_2 - i\tilde{k}_1)} + \frac{\tilde{R}}{2(M-\tilde{k}_2 + i\tilde{k}_1)} + 2\alpha M. \tag{25}$$

By applying the partial fraction decomposition to the last term of Eq. (24), it can be further rewritten as

$$W(z)^2 - 2\tilde{S}'(z)W(z) + \tilde{R}\left(\frac{W(\tilde{k}_2 + i\tilde{k}_1)}{z-\tilde{k}_2 - i\tilde{k}_1} + \frac{W(\tilde{k}_2 - i\tilde{k}_1)}{z-\tilde{k}_2 + i\tilde{k}_1}\right) + 4\alpha = 0. \tag{26}$$

Therefore, the solution is given by

$$W(z) = \tilde{S}'(z) - \left\{\tilde{S}'(z)^2 - \left[\tilde{R}\left(\frac{W(\tilde{k}_2 + i\tilde{k}_1)}{z-\tilde{k}_2 - i\tilde{k}_1} + \frac{W(\tilde{k}_2 - i\tilde{k}_1)}{z-\tilde{k}_2 + i\tilde{k}_1}\right) + 4\alpha\right]\right\}^{1/2}. \tag{27}$$

Here, the branch of the square root must be chosen appropriately, as will be explained below.

The solution in Eq. (27) has a complex free parameter $W(\tilde{k}_1 + i\tilde{k}_2)$ ($W(\tilde{k}_1 - i\tilde{k}_2)$ is its complex conjugate.). The parameter has to be tuned so that the solution becomes consistent with the expected properties of $W(z)$ defined in Eq. (19): $W(z)$ has the asymptotic behavior $W(z) \sim 1/z$ for $z \to \infty$; singularities (actually cuts) are only on the real axis. One can check that the asymptotic behavior and the absence of poles of $\tilde{S}'(z)$ in $W(z)$ are automatically satisfied by the solution in Eq. (27) with an appropriate choice of the branch of the square root. However, it is difficult to tune $W(\tilde{k}_1 + i\tilde{k}_2)$ so that all the branch cuts of Eq. (27) are located only on the real axis. This is because the content of the square root in Eq. (27) is expressed as a sixth-order polynomial function of z over a common denominator, and the dependence of its zeros on $W(\tilde{k}_1 + i\tilde{k}_2)$ is too complicated to analyze. Therefore, we rather take a different strategy to determine $W(z)$, which will be explained below. Whether a solution by the method below corresponds to the solution in Eq. (27) with a value of $W(\tilde{k}_1 + i\tilde{k}_2)$ can be checked afterwards for each solution.

From the discussions about the possible eigenvalue distributions in Sect. 3 and Eq. (20), we expect $W(z)$ to have one or two branch cuts on the real axis. From the form of $\tilde{S}'(z)$, we can assume the following forms of $W(z)$. For cases (I), (II), or (IV) in Sect. 3, we assume a one-cut solution,

$$W(z) = \tilde{S}'(z) - \left(\frac{c}{z - \tilde{k}_2 - i\tilde{k}_1} + \frac{c^*}{z - \tilde{k}_2 + i\tilde{k}_1} + 2\alpha \right) \sqrt{z - c_+}\sqrt{z - c_-}, \tag{28}$$

where c is generally complex, c_- and c_+ are real with $c_- < c_+$, and the square roots are taken in the principal branch. From Eq. (20), $\rho(x)$ is non-zero in the region $c_- < x < c_+$. For case (III), we assume a two-cut solution,

$$W(z) = \tilde{S}'(z) - \frac{2\alpha(z - c)}{(z - \tilde{k}_2)^2 + \tilde{k}_1^2} \sqrt{z - c_1}\sqrt{z - c_2}\sqrt{z - c_3}\sqrt{z - c_4}, \tag{29}$$

where the parameters are assumed to be all real and satisfy $c_1 < c_2 < c < c_3 < c_4$, and the square roots are taken in the principal branch. From Eq. (20), the eigenvalue density $\rho(x)$ is non-zero in the two regions $[c_1, c_2]$ and $[c_3, c_4]$. The reason for imposing $c_2 < c < c_3$ is that this condition is necessary for $\rho(x)$ to be positive in both these regions.

For the expressions in Eqs. (28) and (29), it is straightforward to write down the conditions for the absence of singularities except on the real axis and the asymptotic behavior $W(z) \sim 1/z$ in $z \to \infty$. For the one-cut solution in Eq. (28), we obtain

$$\begin{aligned}
&\tilde{R}/2 - c\sqrt{\tilde{k}_2 + i\tilde{k}_1 - c_+}\sqrt{\tilde{k}_2 + i\tilde{k}_1 - c_-} = 0, \\
&-\alpha(c_+ + c_-) + c + c^* = 0, \\
&\tilde{R} + (c + c^*)(c_+ + c_-)/2 + \alpha(c_+ - c_-)^2/4 - c(\tilde{k}_2 + i\tilde{k}_1) - c^*(\tilde{k}_2 - i\tilde{k}_1) = 1.
\end{aligned} \tag{30}$$

The first condition comes from that $W(z)$ should not inherit the poles of $\tilde{S}'(z)$, since they are at complex values $z = k_2 \pm ik_1$. The second and the third conditions are for the asymptotic behavior of $W(z)$ to be $\sim 1/z$. Since the number of conditions and the number of free parameters are the same, the solution is uniquely determined (there may exist some discrete sets of solutions, though).

For the two-cut solution in Eq. (29), we first perform a replacement of the argument $z - \tilde{k}_2 = y$ for simplicity, and parameterize $W(z)$ as

$$W(y) = \tilde{S}'(y + \tilde{k}_2) - \frac{2\alpha(y - d)}{y^2 + \tilde{k}_1^2} \sqrt{y - d_1}\sqrt{y - d_2}\sqrt{y - d_3}\sqrt{y - d_4}, \tag{31}$$

where $d = c - \tilde{k}_2$ and so on, and $d_1 < d_2 < d < d_3 < d_4$. We obtain

$$\begin{aligned}
&\frac{\tilde{R}}{2} - \frac{\alpha(i\tilde{k}_1 - d)}{i\tilde{k}_1} \prod_{l=1}^{4} \sqrt{i\tilde{k}_1 - d_l} = 0, \\
&\tilde{k}_2 + d + \frac{1}{2}\sum_{l=1}^{4} d_l = 0, \\
&\tilde{R} + 2\alpha \left(-\frac{d}{2}\sum_{l=1}^{4} d_l + \tilde{k}_1^2 + \frac{1}{8}\sum_{l=1}^{4} d_l^2 - \frac{1}{4}\sum_{\substack{l,m=1 \\ l<m}}^{4} d_l d_m \right) = 1.
\end{aligned} \tag{32}$$

The first condition is for the absence of the poles of $\tilde{S}'(z)$ in $W(z)$, and the last two are for the asymptotic behavior. The conditions in Eq. (32) give four real conditions in total, since the first is a complex-valued condition and the latter are real. Therefore, the solution has one free parameter, since the number of the parameters in Eq. (29) is five.

The presence of one free parameter in the two-cut solution is physically understandable by the aligned Coulomb gas picture of Sect. 3. There are two bunches of the eigenvalues, between which there exists an infinite potential barrier in the large-N limit. Therefore, part of the eigenvalues can, freely to some extent, be moved between the two bunches without losing the stability of the solution. This freedom gives one free parameter to the solution.

Yet one can fix this freedom by imposing that the two bunches have the same chemical potential [28]. In other words, this condition is that there is no energy cost when moving an eigenvalue from one bunch to the other. This balance between the two bunches is relevant if N is not taken strictly to the infinite. To obtain the condition for the balance, let us take the aligned Coulomb gas picture of Sect. 3. Suppose a particle with a small charge is located at x between the two bunches of particles. Then the force $F(x)$ acting on the particle is proportional to

$$F(x) = W(x) - \tilde{S}'(x), \tag{33}$$

where the first term represents the repulsive Coulomb forces coming from the particles contained in the bunches, and the second the forces from the negative charge and the harmonic potential. Then, the energy cost of moving a particle from one bunch to the other is given by $\int_{c_2}^{c_3} dx\, F(x)$. This should vanish for the balance, and, by using Eq. (29), we obtain

$$\int_{d_2}^{d_3} dy\, \frac{y-d}{y^2+\tilde{k}_1^2}\sqrt{y-d_1}\sqrt{y-d_2}\sqrt{d_3-y}\sqrt{d_4-y} = 0. \tag{34}$$

With this additional condition, the two-cut solution is uniquely determined (there may exist some discrete sets of solutions, though).

Once a solution is obtained, one can compute the eigenvalue density by Eq. (28). We obtain

$$\rho(x) = \frac{1}{\pi}\left(\frac{c}{x-\tilde{k}_2-i\tilde{k}_1} + \frac{c^*}{x-\tilde{k}_2+i\tilde{k}_1} + 2\alpha\right)\sqrt{c_+-x}\sqrt{x-c_-} \tag{35}$$

in the region $[c_-, c_+]$ for the one-cut solution. Note that the positivity of $\rho(x)$ in the one-cut solution is not automatically satisfied, and there actually exist solutions with negative regions of $\rho(x)$ for some parameters. In such a case, the solutions are not correct, and other one-cut or two-cut solutions must be taken for these parameters. For the two-cut solution in Eq. (29), once a solution is found with $c_2 < c < c_3$, the positivity of $\rho(x)$ is automatically satisfied and

$$\rho(x) = \frac{1}{\pi}\frac{2\alpha|x-c|}{(x-\tilde{k}_2)^2+\tilde{k}_1^2}\sqrt{|(x-c_1)(x-c_2)(x-c_3)(x-c_4)|} \tag{36}$$

for the ranges $[c_1, c_2]$ and $[c_3, c_4]$.

5. Examples and a simple case

It seems difficult to obtain explicit solutions to the equations obtained in Sect. 4. In particular, Eq. (34) is an integral equation and would probably not be explicitly solvable. Yet, it is possible to numerically find solutions. To demonstrate, Fig. 2 shows some eigenvalue densities $\rho(x)$ which have been obtained by numerically solving the equations in Sect. 4 for the four cases in Sect. 3.

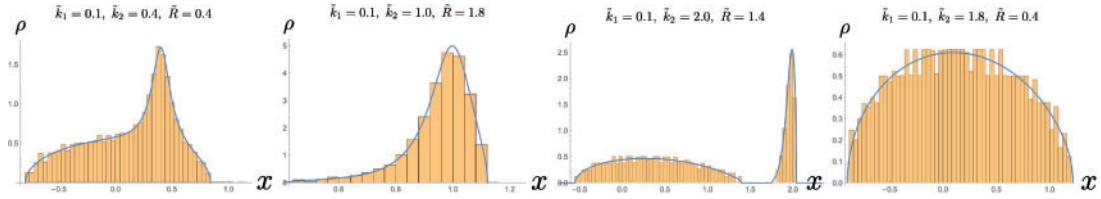

Fig. 2. Examples of eigenvalue densities corresponding to the four cases (I), (II), (III), and (IV), from left to right. The results of the Monte Carlo simulations of the system in Eq. (13) with $N = 200$ are shown by the histograms of λ_a after the rescaling in Eq. (14). The eigenvalue densities $\rho(x)$ obtained by solving the equations in Sect. 4 are shown by the solid lines. We take $\alpha = 1$. There are no clear qualitative differences between cases (I) and (II) of the examples.

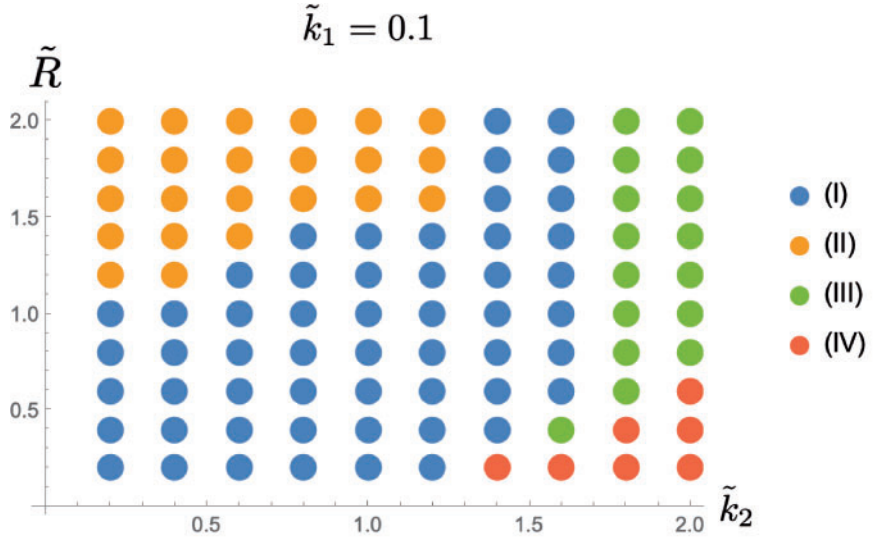

Fig. 3. Classification of the data points into cases (I)–(IV) by the histograms of λ_a for $\tilde{k}_1 = 0.1$ and $\alpha = 1$. The points are taken with interval 0.2 in the square region, $0.2 \leq \tilde{k}_2 \leq 2.0$ and $0.2 \leq \tilde{R} \leq 2.0$. The histograms of λ_a are obtained from the Monte Carlo simulation of the Coulomb gas system for each point of the parameters with $N = 200$. A point to note is that the boundary between (I) and (II) is rather arbitrary, because of the lack of a clear distinction between the two profiles.

These are consistent with the results obtained from the Monte Carlo simulations of the aligned Coulomb gas system with $N = 200$ in Sect. 3, as shown by the histograms of λ_a after the rescaling in Eq. (14). We can see that there are no clear qualitative differences between the profiles of cases (I) and (II), and therefore the classifications into (I) or (II) are rather arbitrary in the examples.

In Fig. 3, the phase structure is shown in the plane of $(\tilde{k}_2, \tilde{R})$ for $\tilde{k}_1 = 0.1$ and $\alpha = 1$. This is obtained by classifying the histograms of λ_a obtained from the Monte Carlo simulations of the system in Eq. (13) with $N = 200$. We see that the four cases discussed in Sect. 3 do indeed exist. A point to note in this figure is that the boundary between cases (I) and (II) is rather arbitrary, since the profiles of (I) and (II) cannot clearly be distinguished.

Although the distinction between cases (I) and (II) is not clear in the examples above, one can find a reason for separating the two cases in the limit $\tilde{k}_1 \to +0$. To see this, let us consider the explicitly solvable case by putting $\tilde{k}_2 = 0$. This case corresponds to the one-cut solution, and the conditions

in Eq. (30) can straightforwardly be solved. The result of $\rho(x)$ is given by

$$\rho(x) = \frac{1}{\pi}\left(\frac{\tilde{R}\,\tilde{k}_1}{(x^2+\tilde{k}_1^2)\sqrt{\tilde{k}_1^2+a^2}} + 2\alpha\right)\sqrt{a^2-x^2}, \tag{37}$$

where $a := c_+ = -c_- > 0$, and is determined by

$$\tilde{R} - \frac{\tilde{R}\tilde{k}_1}{\sqrt{\tilde{k}_1^2+a^2}} + \alpha\, a^2 = 1. \tag{38}$$

Since the left-hand side is a monotonically increasing function of a with 0 at $a = 0$ and $+\infty$ at $a = +\infty$, there always exists a unique solution of $a > 0$ to the equation. One can also show that, by taking partial derivatives of the left-hand side with respect to the variables, there exists no singular behavior of a as a function of $\tilde{k}_1$ and $\tilde{R}$. This is consistent with the statement above that cases (I) and (II) cannot be absolutely distinguished. However, let us take the $\tilde{k}_1 \to +0$ limit. In this case, the solution to Eq. (38) is explicitly given by

$$a = \begin{cases} \sqrt{(1-\tilde{R})/\alpha}, & \tilde{R} < 1, \\ 0, & \tilde{R} \geq 1. \end{cases} \tag{39}$$

A singularity appears at $\tilde{R} = 1$. Hence, after taking the limit $\tilde{k}_1 \to +0$, (I) and (II) can clearly be distinguished by the order parameter a. In the next section we will more thoroughly study the limit $\tilde{k}_1 \to +0$.

6. The $\tilde{k}_1 \to +0$ limit

While it does not seem possible to obtain explicit solutions to the equations in Sect. 4 for general values of the parameters, we can obtain explicit solutions by taking the $\tilde{k}_1 \to +0$ limit. Fortunately, this limit is exactly consistent with our main purpose, namely, studying the case corresponding to the positive cosmological constant case of CTM, as explained in Sect. 2. We obtain explicit solutions for cases (I), (II), and (III). Case (IV) disappears in this limit, because the potential generated by the $-R$ charge becomes infinitely deep, and there always exist a bunch of eigenvalues around it.

Let us first consider case (I). We assume $\tilde{R} < 1$ and $c_- < \tilde{k}_2 < c_+$ for the one-cut solution. The last assumption and $\tilde{k}_1 \to +0$ leads to $\sqrt{\tilde{k}_2 + i\tilde{k}_1 - c_+}\sqrt{\tilde{k}_2 + i\tilde{k}_1 - c_-} = i\sqrt{c_+ - \tilde{k}_2}\sqrt{\tilde{k}_2 - c_-}$ in the first equation of Eq. (30), and therefore c must be pure imaginary. Then the second equation leads to $c_+ + c_- = 0$ in the limit. Finally, with the third equation, we obtain

$$\begin{aligned} c &= -\frac{i\tilde{R}}{2\sqrt{c_+ - \tilde{k}_2}\sqrt{\tilde{k}_2 - c_-}}, \\ c_\pm &= \pm\sqrt{\frac{1-\tilde{R}}{\alpha}} \end{aligned} \tag{40}$$

in the limit. Note that, because of the assumption $c_- < \tilde{k}_2 < c_+$, this solution is consistent only if

$$1 - \tilde{R} - \alpha\tilde{k}_2^2 > 0. \tag{41}$$

By putting the solution in Eq. (40) into Eq. (35), $\rho(x)$ is obtained as

$$\begin{aligned}\rho_{(\mathrm{I})}(x) &= \lim_{\tilde{k}_1\to+0}\frac{1}{\pi}\frac{\tilde{R}\,\tilde{k}_1}{(x-\tilde{k}_2)^2+\tilde{k}_1^2}+\frac{2\alpha}{\pi}\sqrt{(1-\tilde{R})/\alpha-x^2}\\ &= \tilde{R}\,\delta(x-\tilde{k}_2)+\frac{2\alpha}{\pi}\sqrt{(1-\tilde{R})/\alpha-x^2},\end{aligned} \tag{42}$$

where the domain of x is restricted to the positive region of the square root. One can check that $\int_{\mathbb{R}} dx\rho_{(\mathrm{I})}(x) = 1$ holds.

The result in Eq. (42) can intuitively be understood by the aligned Coulomb gas picture discussed in Sect. 3. In the $\tilde{k}_1 \to +0$ limit, the potential generated by the charge $-R$ at $x = \tilde{k}_2$ becomes infinitely deep, and some of the particles of unit charge are trapped at the location $x = \tilde{k}_2$ in the limit. When $\tilde{R} < 1$, i.e. $N > R$, the number of particles trapped is equal to R, since the particles are trapped until the $-R$ charge is totally screened. This concentration of particles is represented by the first term of Eq. (42). Because of the total screening, the $-R$ charge is totally hidden from the remaining $N-R$ particles of unit charge, and therefore they form the semicircle distribution because of the harmonic potential, as represented by the second term of Eq. (42).

Let us next consider $\tilde{R} > 1$. In this case, since $N < R$, the $-R$ charge at $x = \tilde{k}_2$ can only be partially screened. This means that all the particles of unit charge are concentrated around $x = \tilde{k}_2$ in the limit $\tilde{k}_1 \to +0$, which corresponds to case (II) of Sect. 3. Therefore, we may naturally assume the behavior

$$\begin{aligned}c_+ &\sim \tilde{k}_2 + b_+\tilde{k}_1,\\ c_- &\sim \tilde{k}_2 - b_-\tilde{k}_1\end{aligned} \tag{43}$$

in the $\tilde{k}_1 \to +0$ limit, where $b_-, b_+ > 0$. Putting the assumption in Eq. (43) into the first equation of Eq. (30), we obtain

$$c \sim -\frac{i\tilde{R}}{2\tilde{k}_1\sqrt{b_+ - i}\sqrt{b_- + i}} \tag{44}$$

as the behavior for $\tilde{k}_1 \to +0$. By putting the assumption in Eq. (43) into the second equation of Eq. (30), we see that the real part of c does not diverge in the limit:

$$c + c^* \sim 2\alpha\tilde{k}_2. \tag{45}$$

Therefore, this requires $b_+ = b_-$ in Eq. (44). By noting that $(c + c^*)(c_+ + c_- - 2\tilde{k}_2)$ has lower order than $\tilde{k}_1$, the third equation of Eq. (30) leads to

$$b_\pm = \frac{\sqrt{2\tilde{R}-1}}{\tilde{R}-1}, \tag{46}$$

where $b_\pm := b_+ = b_-$. By putting the results into Eq. (35), we obtain

$$\rho_{(\mathrm{II})}(x) = \lim_{\tilde{k}_1\to+0}\frac{(\tilde{R}-1)\sqrt{(b_\pm\tilde{k}_1)^2-(x-\tilde{k}_2)^2}}{\pi((x-\tilde{k}_2)^2+\tilde{k}_1^2)} = \delta(x-\tilde{k}_2), \tag{47}$$

where the domain of x in the middle expression is the positive region of the square root.

Let us next consider the two-cut solution in the $\tilde{k}_1 \to +0$ limit. Since the potential generated by the $-R$ charge becomes infinitely deep, case (III) with $N > R$ ($\tilde{R} < 1$) is the only possibility, and case (IV) does not appear. In a similar spirit to above, it is natural to assume the behavior for $\tilde{k}_1 \to +0$ as

$$\begin{aligned} d_1 &\sim -b_1, \\ d_2 &\sim -b_2, \\ d_3 &\sim -b_0\tilde{k}_1, \\ d_4 &\sim b_0\tilde{k}_1, \\ d &\sim -b, \end{aligned} \tag{48}$$

where b, b_i are all positive. Here, one may start by assuming different proportional coefficients for d_3 and d_4, but they turn out to be the same by the equations, as we encountered in the previous case. The ordering of the d's restricts $0 < b < b_2 < b_1$. By putting the assumptions into Eq. (32), we obtain

$$\begin{aligned} &\tilde{R} = 2\alpha b\sqrt{b_1 b_2(1+b_0^2)}, \\ &\tilde{k}_2 - b - (b_1+b_2)/2 = 0, \\ &\tilde{R} + \alpha\left(-b(b_1+b_2) + (b_1-b_2)^2/4\right) = 1 \end{aligned} \tag{49}$$

in the limit. Solving these equations, we obtain

$$\begin{aligned} b_0 &= \sqrt{\tilde{R}^2/(4\alpha^2 b^2 b_1 b_2) - 1}, \\ b_1 &= \tilde{k}_2 - b + \sqrt{(1-\tilde{R})/\alpha + 2b(\tilde{k}_2 - b)}, \\ b_2 &= \tilde{k}_2 - b - \sqrt{(1-\tilde{R})/\alpha + 2b(\tilde{k}_2 - b)}. \end{aligned} \tag{50}$$

As discussed below Eq. (32), the solution in Eq. (50) has one free parameter, which may be chosen to be b. It is not totally free and is restricted to a range. One condition comes from the ordering $0 < b < b_2$ mentioned above, which leads to

$$0 < b < \frac{1}{2}\tilde{k}_2 - \left\{\frac{1}{6}\left(\frac{1}{2}\tilde{k}_2^2 + \frac{1-\tilde{R}}{\alpha}\right)\right\}^{1/2}. \tag{51}$$

Note that the presence of this region requires

$$\alpha\tilde{k}_2^2 - 1 + \tilde{R} > 0. \tag{52}$$

Another condition comes from b_0 being real in Eq. (50), which requires $\tilde{R}^2 > 4\alpha^2 b^2 b_1 b_2$. To see what this inequality requires, let us introduce a function of b, $g(b) := 4\alpha^2 b^2 b_1 b_2$, where b_1, b_2 are given by the expressions depending on b in Eq. (50). Then we find its derivative to be

$$g'(b) = 4\alpha^2\left(12(b - \tilde{k}_2/2)^2 - \tilde{k}_2^2 - 2(1-\tilde{R})/\alpha\right) > 0, \tag{53}$$

where the positivity comes from Eq. (51). Since $g(0) = 0$, the condition $\tilde{R}^2 > 4\alpha^2 b^2 b_1 b_2$ may also give an additional bound of the form $0 < b < b_{\max}$ with $g(b_{\max}) = \tilde{R}^2$. Though the bound is not

explicitly determined, an important point here is that there exists a finite range of b for a solution, if the condition in Eq. (52) is satisfied.

By putting Eqs. (48) and (50) into Eq. (36), and taking the $\tilde{k}_1 \to +0$ limit, one obtains

$$\rho_{(\mathrm{III})}(x) = \frac{2\alpha(x+b-\tilde{k}_2)\sqrt{(x+b_1-\tilde{k}_2)(-x-b_2+\tilde{k}_2)}}{\pi(x-\tilde{k}_2)} + \tilde{R}\left(1-\frac{1}{\sqrt{1+b_0^2}}\right)\delta(x-\tilde{k}_2), \quad (54)$$

where the domain of x for the first term is restricted to the positive region of the square root. One can check the normalization, $\int dx \rho_{(\mathrm{III})}(x) = 1$.

We can also take into account the condition in Eq. (34) for the balance of the chemical potential between the two bunches. In the $\tilde{k}_1 \to +0$ limit, the condition gives

$$\begin{aligned} d &= \frac{\int_{d_2}^{d_3} dy \, \frac{y}{y^2+\tilde{k}_1^2}\sqrt{y-d_1}\sqrt{y-d_2}\sqrt{d_3-y}\sqrt{d_4-y}}{\int_{d_2}^{d_3} dy \, \frac{1}{y^2+\tilde{k}_1^2}\sqrt{y-d_1}\sqrt{y-d_2}\sqrt{d_3-y}\sqrt{d_4-y}} \\ &\sim \frac{\int_{d_2}^{d_3} dy \sqrt{y-d_1}\sqrt{y-d_2}}{\int_{d_2}^{d_3} dy \, \frac{1}{y}\sqrt{y-d_1}\sqrt{y-d_2}} \to 0, \end{aligned} \quad (55)$$

because $d_3, d_4 \to 0$, where we assume $d_2 = -b_2$ is finitely below zero in the limit; we will see its consistency below. By setting $b = -d \to +0$ in Eq. (50), we obtain

$$\begin{aligned} &b_0 \to +\infty, \\ &b_1 = \tilde{k}_2 + \sqrt{(1-\tilde{R})/\alpha}, \\ &b_2 = \tilde{k}_2 - \sqrt{(1-\tilde{R})/\alpha}. \end{aligned} \quad (56)$$

For this solution, the eigenvalue distribution is given by

$$\rho_{(\mathrm{III})}^{\mathrm{balance}}(x) = \frac{2\alpha\sqrt{(1-\tilde{R})/\alpha - x^2}}{\pi} + \tilde{R}\,\delta(x-\tilde{k}_2), \quad (57)$$

where the domain of x for the first term is restricted to the positive region of the square root. We again obtain the distribution of the semicircle law and the concentration at $x = \tilde{k}_2$.

The condition in Eq. (52) for the presence of a solution for case (III) is a complement to Eq. (41) for case (I). Therefore, there is a transition line,

$$\alpha\tilde{k}_2^2 - 1 + \tilde{R} = 0, \quad (58)$$

between the two phases (I) and (III). Collecting the results in this section, the phase structure in the $\tilde{k}_1 \to +0$ limit is given in Fig. 4.

7. Implications for the canonical tensor model

The wave function in Eq. (A.3) [17] of the CTM [14,15] has the interesting property that the peaks of the wave function are located at the configurations (the values of the tensor P_{abc}) which are invariant under Lie group symmetries [18,19]. This property is particularly interesting from the perspective of spacetime emergence in CTM, because this property would provide a natural mechanism for

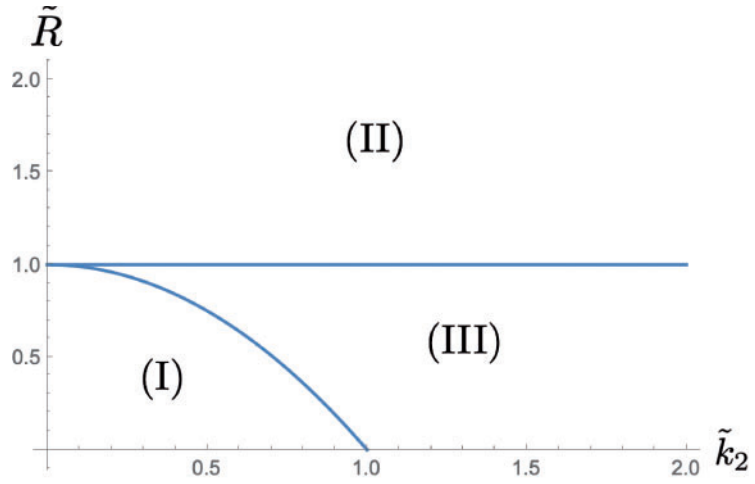

Fig. 4. The phase structure in the $\tilde{k}_1 \to +0$ limit with $\alpha = 1$.

spacetime emergence by generating spacetimes as representation spaces of Lie groups. However, this property has not been fully studied because of some technical difficulties, as explained in Sects. 1 and 2. This gives the main motivation for studying the particular simplified model in Eq. (1) of a matrix, which is derived from a matrix analogue of the wave function of CTM.

The relation between peaks and symmetries is simple in the matrix model of Eq. (1). The real symmetric M_{ab} becomes Lie group symmetric when and only when n of the eigenvalues take the same values, in which $SO(n)$ is the Lie group symmetry.[6] In the aligned Coulomb gas picture of Sect. 3, this corresponds to n of the particles of unit charge being concentrated at a location. In fact, in the $\tilde{k}_1 \to +0$ limit, R (or N if $N < R$) of the particles concentrate at $x = \tilde{k}_2$ to screen the $-R$ charge there, as has explicitly been derived in Sect. 4. Therefore, we see the emergence of $SO(R)$ (or $SO(N)$ if $N < R$) symmetry in the matrix model in the $\tilde{k}_1 \to +0$ limit.

The above discussions do not depend on the value of $\tilde{k}_2$. However, we have two different phases, (I) and (III), on the same value of $\tilde{R} < 1$, as shown in Fig. 4. In fact, there is a qualitative difference between (I) and (III) concerning the symmetry emergence.

To see this in the following discussions, let us assume that $\tilde{k}_1$ is very small, $\tilde{k}_1 \ll 1$, but the limit $\tilde{k}_1 \to +0$ is not strictly taken. It would still be meaningful to discuss the symmetry enhancement above in an approximate sense, though the concentration of the eigenvalues is not exactly on $\tilde{k}_2$ anymore. Let us first note that, in phase (I), all the eigenvalues are continuously distributed, and there are no clear boundaries between the eigenvalues near $\tilde{k}_2$ and those which are not. Therefore, the number n of eigenvalues near $\tilde{k}_2$ is ambiguous, meaning that the enhanced symmetry is ambiguous in this phase. Moreover, by adding perturbations to the system, it would be possible to smoothly move some of the eigenvalues toward or away from $\tilde{k}_2$. Therefore, the enhanced symmetry can easily be changed under perturbations. The situation is illustrated in the left panel of Fig. 5.

On the other hand, in phase (III), the bunch of eigenvalues around $\tilde{k}_2$ is separated from the other bunch of eigenvalues. In fact, there exists a potential barrier (infinite in the large-N limit) for eigenvalues to move between the two bunches (the necessary force is proportional to Eq. (33); see Fig. 6 for an illustration). Therefore, in phase (III), the symmetry associated with an eigenvalue distribution

[6] We may also consider the possibilities of concentrations to multiple values, but this does not occur in the present matrix model, in which only a concentration at $x = \tilde{k}_2$ can occur.

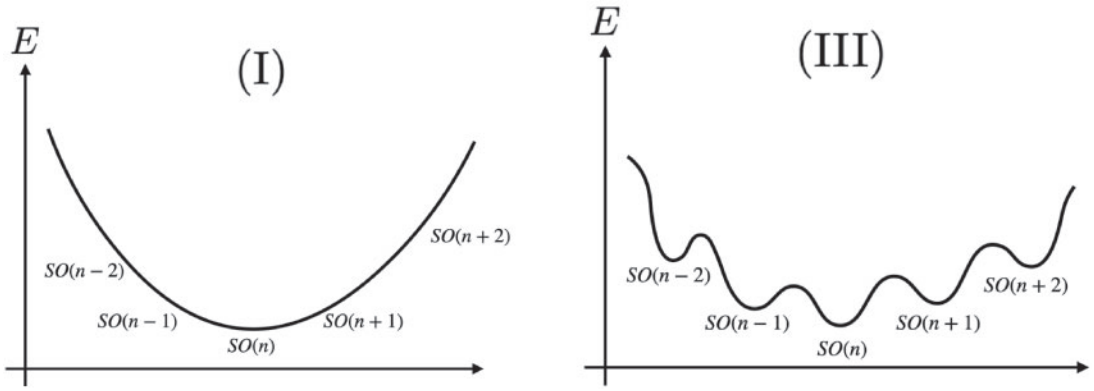

Fig. 5. An illustration of the difference between phases (I) and (III) concerning symmetry. In phase (I), the symmetry associated with an eigenvalue distribution is ambiguous and is subject to changes under perturbations. In phase (III), symmetries are definite and stable against perturbations. In (III) there are metastable states with other symmetries.

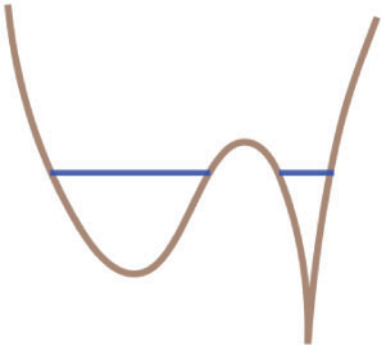

Fig. 6. Illustration of the potential and the chemical potential corresponding to case (III). There is a potential barrier between the two bunches of eigenvalues. The chemical potentials of the two bunches take the same value in the figure. If some of the eigenvalues are moved between the bunches, the chemical potentials get unbalanced, corresponding to metastable states.

is definite and is stable against perturbations. There are also metastable states which correspond to distributions obtained by moving some of the eigenvalues from one bunch to the other. Other symmetries are associated with these metastable states, since the numbers of eigenvalues in the bunch around $\tilde{k}_2$ are different. The situation is illustrated in the right panel of Fig. 5.

Let us now move on to the discussions on the emergent spaces associated with the symmetries. To see this, let us go back to the origin of the matrix model in Eq. 3. It is clear from the expression that the distribution of ϕ_a extends to the directions of the eigenvectors of M_{ab} whose eigenvalues are near k_2. In other words, when M_{ab} has n eigenvalues near k_2, the distribution of ϕ_a forms an n-dimensional ball B^n with a radius of order $1/\sqrt{k_1}$. The differences between the other eigenvalues and k_2 determine the transverse sizes (the thickness) of the ball. The ball gives the representation space of the $SO(n)$ symmetry. Here, it is important that the emergent spaces are realized by distributions of ϕ_a, rather than ϕ_a itself, which transforms under $SO(n)$. More explanations will be given at the end of this section on this point.

We again encounter an ambiguity in phase (I). The sizes of some of the transverse directions (the thickness) of the ball B^n are actually similar to that of B^n, and therefore the dimension of the ball is

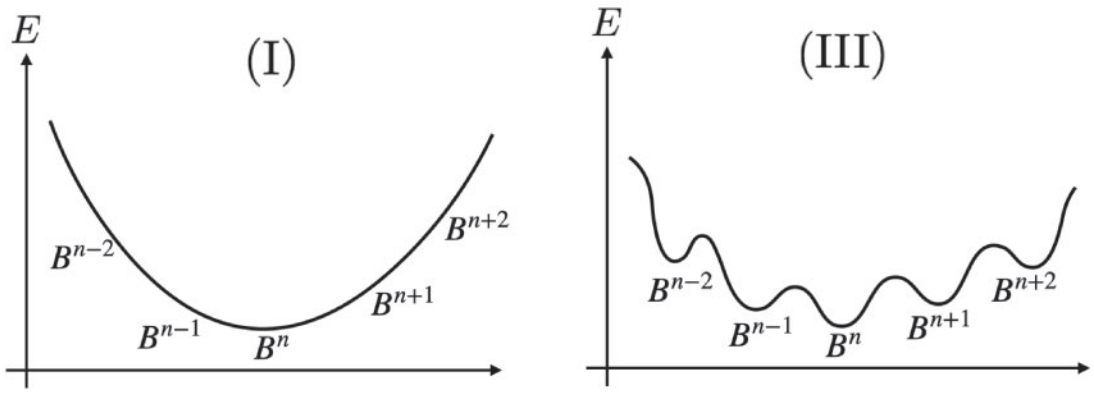

Fig. 7. Illustration of the difference between phases (I) and (III) concerning the dimension of an emergent space, an n-dimensional ball B^n. In phase (I), the dimension is ambiguous and is subject to changes by perturbations. In phase (III), the dimension is definite and stable against perturbations. There are metastable states representing other dimensional balls in phase (III).

ambiguous. In addition, the dimension is subject to changes by perturbations. On the other hand, in phase (III), the dimension is well determined, because the clear distinction between the eigenvalues of M_{ab} which are near k_2 and those which are not provides a hierarchy of sizes between the ball B^n and its transverse directions. The dimension is also stable against perturbations. The situation is described in Fig. 7.

Another major outcome from the matrix model is that this gives some indirect support to the previous Monte Carlo results for CTM [21–23]. Here, as explained in Sects. 1 and 2, the previous numerical results are for the negative cosmological constant, corresponding to $k_2 = 0$ in the matrix model. An important previous result is that we found a continuous phase transition point near[7] $2R \sim N^2/2$. This was observed for large N and small k, which corresponds to k_1 in the matrix model. This transition point seems to correspond to the singular point of the matrix model found at $R = N$ in the limit $\tilde{k}_1 = k_1/N \to +0$, which was discussed in the final part of Sect. 5. If we identify them as similar kinds of points, the phase diagram of the matrix model shown in Fig. 4 suggests that the transition point found for CTM in the previous Monte Carlo studies is a common endpoint of phase transition lines which extend into the parameter region of positive cosmological constants. This gives a strong motivation for the future study of CTM for the positive cosmological constant case, because the transition lines in the matrix model are the boundary of phase (III), which is important for stable symmetries/dimensions of emergent spaces.

The R dependence shown above of the symmetries and dimensions of the distributions of ϕ_a in the matrix model seems to parallel the R dependence observed for CTM in Refs. [21–23]. However, there exists a crucial difference. In the matrix model, the dimension increases with R, reaches its maximum around $R = N$ (see the left panel of Fig. 8). On the other hand, in CTM, the dimension takes a minimum at the critical point (see the right panel of Fig. 8). Currently, we do not understand this difference.

Lastly, we provide more explanation about the emergent spaces in the above context. To do this, let us look at the expression in Eq. (6), which represents the wave function $\Psi(M)$ with R replicas. Let us assume that k_1 is very small and that n of the eigenvalues of M are very close to k_2, while the others

[7] There is a difference in the definition of R by a factor of 2 between the present and previous papers for the convenience of each: $2R$ in this paper corresponds to R in Refs. [20–23].

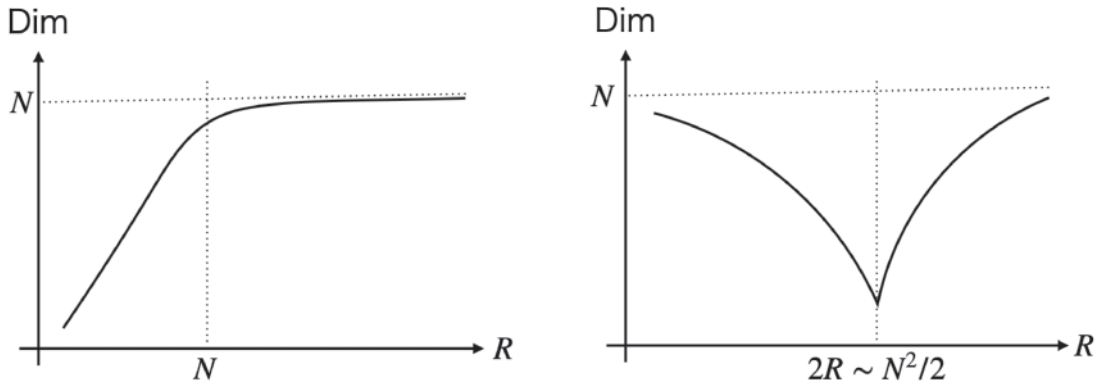

Fig. 8. Illustrations of the R dependencies of the dimensions of the distributions of ϕ_a for the matrix (left) and CTM (right) cases. The right behavior was obtained in Ref. [22].

are significantly different from k_2. Then, it is clear from the expression in Eq. (6) that dominant contributions of integrations over ϕ_a^l come from the configurations where all ϕ_a^l ($l = 1, 2, \ldots, R$) lie in the vicinity of the linear subspace over the eigenvectors of M for the n eigenvalues close to k_2. This is an n-dimensional ball of size $\sim 1/\sqrt{k_1}$. In fact, the presence of such a ball of dominance can be detected by studying the probability distribution of an $SO(N)$-invariant observable like $\phi_a^i \phi_a^j / |\phi^i||\phi^j|$ ($i < j$). This observable[8] detects the mutual azimuthal angles θ among the vectors ϕ^i ($i = 1, 2, \ldots, R$) in the N-dimensional space, and the probabilistic distribution $\rho(\theta)\, d\theta$ of the angles should obey $\propto \sin^{n-2}(\theta)\, d\theta$, which represents the area elements on the $(n-1)$-dimensional unit sphere. Because of the $SO(N)$ invariance of the observable, the dimension n extracted by this procedure is a meaningful quantity even in the matrix model, i.e. even after making M_{ab} dynamical, if fluctuations of n are negligible, as in the large-N limit in the preceding sections. Indeed, one would be able to compute expectation values of arbitrary products of the observable in the matrix model.

8. Summary and future prospects

We have studied a matrix model derived from a matrix analogue to the wave function of the canonical tensor model, and have shown that positivity of the cosmological constant is vital for the presence of emergent spaces with stable symmetries and dimensions.

More precisely, we have studied a one-matrix model of a real symmetric matrix with a potential which is a sum of two logarithmic functions and a quadratic one. This is a simplified toy model obtained by replacing the tensor argument of the wave function [17] of CTM [14,15] with a matrix and considering the absolute square norm of the wave function. The main purpose of the present study is to foresee the possible outcomes of CTM for the positive cosmological constant case by studying the toy matrix model for the corresponding case. The properties of CTM for the positive cosmological constant case have not been studied in the previous numerical works [21–23] because of some technical difficulties: the quantity we need to compute is oscillatory for the positive cosmological constant case, suffering from the sign problem of Monte Carlo simulations. This paper has shown that, in the matrix model, positivity of the cosmological constant is vital for the presence of a phase

[8] This kind of observable is called an overlap and they often appear in spin glass theory [30]. This was also used to study dimensions of dominant configurations in Ref. [22] with Monte Carlo simulations.

in which symmetries and dimensions of emergent spaces are definite and stable. This result would strongly encourage the future study of the positive cosmological constant case in CTM.

The matrix model has been shown to have a critical point at $R = N$ for $k_2 = 0$ in the limit $\tilde{k}_1 = k_1/N \to +0$, as discussed at the end of Sect. 5. A similar critical point has been found for CTM at $2R \sim N^2/2$ in Refs. [20–23]. Therefore, the analytical result of the matrix model has given indirect confirmation of the numerical Monte Carlo result in Refs. [21–23]. However, there exists a crucial difference between the two critical points concerning the dimensional behaviors in R, as discussed in Sect. 7 (see Fig. 8). This difference should be studied more deeply, since it will be directly linked to the mechanism of the emergent phenomena in CTM.

Though the matrix model presented in this paper does not fully describe the properties of CTM, it gives intriguing insights for future CTM analysis. For instance, the importance of the eigenvalue density profiles for the dynamics of emergent spaces in the matrix model motivates the study of CTM in the light of the tensor eigenvalue/vector problem [31]. Various other aspects, such as thermodynamic properties, of the matrix model remain unexplored, which are also expected to give some insights into CTM. The matrix model would also provide an arena for developing tools to efficiently analyze CTM.

Acknowledgements

The work of N.S. is supported in part by Japan Society for the Promotion of Science (JSPS) KAKENHI Grant No. 19K03825.

Funding

Open Access funding: SCOAP[3].

Appendix A. A minimal introduction to CTM

We provide here minimal information about the canonical tensor model (CTM) in order for readers to understand the connection between CTM and the matrix model in Eq. (1). A more thorough but concise summary of CTM can be found in an appendix of Ref. [21].

CTM [14,15] is a tensor model formulated as a first-class constrained system in the Hamilton formalism. Its dynamical variables are a canonical conjugate pair of real symmetric three-index tensors, Q_{abc} and P_{abc} $(a, b, c = 1, 2, \ldots, N)$, and there are two kinds of first-class constraints $\mathcal{H}_a$ and $\mathcal{H}_{ab}$ $(= -\mathcal{H}_{ba})$, which form a closed Poisson algebra with dynamical-variable-dependent structure coefficients. The canonical quantization of CTM is straightforward [16], and the physical state condition is given by $\hat{\mathcal{H}}_a|\Psi\rangle = \hat{\mathcal{H}}_{ab}|\Psi\rangle = 0$, where $\hat{\mathcal{H}}_a$ and $\hat{\mathcal{H}}_{ab}$ are the quantized constraints. The explicit form of $\hat{\mathcal{H}}_a$ is given by

$$\hat{\mathcal{H}}_a = \hat{P}_{abc}\hat{P}_{bde}\hat{Q}_{cde} - \lambda\,\hat{Q}_{abb} + i\,\lambda_H\,\hat{P}_{abb}, \tag{A.1}$$

where λ is identified with the cosmological constant of general relativity (GR) from the equivalence between the $N = 1$ CTM and the minisuperspace approximation of GR [32]. λ_H is uniquely determined by the hermiticity of $\hat{\mathcal{H}}_a$ as $\lambda_H = (N + 2)(N + 3)/2$. The wave function which represents the exactly solved physical state is given by

$$\Psi_{\mathrm{CTM}}(P) := \langle P|\Psi\rangle = \varphi_{\mathrm{CTM}}(P)^{\lambda_H/2}, \tag{A.2}$$

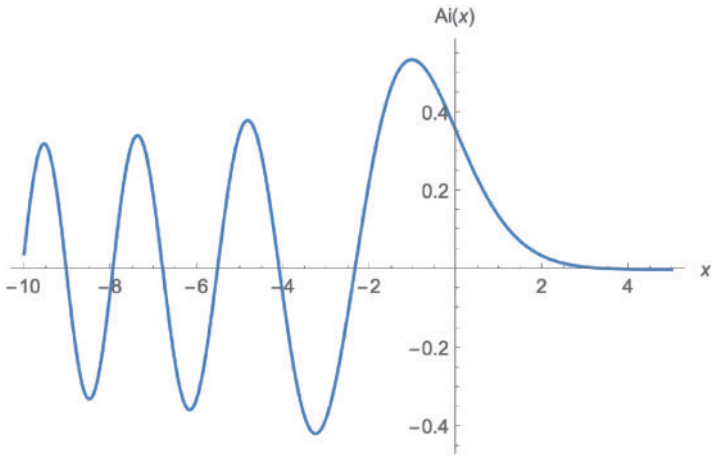

Fig. A.1. The Airy Ai function.

where

$$\varphi_{\rm CTM}(P) := \int_{\mathcal{C}} d\tilde{\phi} \prod_{a=1}^{N} d\phi_a \, \exp\left[iP_{abc}\phi_a\phi_b\phi_c - i\,k\,\phi^2\tilde{\phi} + i\,\tilde{\phi}^3/3 \right]. \tag{A.3}$$

Here, k has the same sign as the cosmological constant, because $\lambda \propto k^3$. The integration contour $\mathcal{C}$ can be taken in various ways with an infinite extent as far as the integration converges. We consider the naive choice $\mathcal{C} = \mathbb{R}^{N+1}$ with a regularization, which can, for example, be taken as the one in Ref. [19].[9]

The integration over $\tilde{\phi}$ in Eq. (A.3) provides the expression

$$\varphi_{\rm CTM}(P) = \text{const.} \int_{\mathbb{R}^D} \prod_{a=1}^{N} d\phi_a \, \exp\left(iP_{abc}\phi_a\phi_b\phi_c\right) \mathrm{Ai}(-k\,\phi^2), \tag{A.4}$$

where $\mathrm{Ai}(\cdot)$ denotes the Airy Ai function. For $k > 0$ corresponding to a positive cosmological constant, $\mathrm{Ai}(-k\,\phi^2)$ is an oscillatory function of ϕ^2, while, for $k < 0$ corresponding to a negative cosmological constant, this is a damping function of ϕ^2 (see Fig. A.1).

References

[1] M. Reuter and F. Saueressig, *Quantum Gravity and the Functional Renormalization Group: The Road towards Asymptotic Safety* (Cambridge University Press, Cambridge, 2019).
[2] R. Loll, Class. Quantum Grav. **37**, 013002 (2020) [arXiv:1905.08669 [hep-th]] [Search INSPIRE].
[3] C. Rovelli and F. Vidotto, *Covariant Loop Quantum Gravity: An Elementary Introduction to Quantum Gravity and Spinfoam Theory* (Cambridge University Press, Cambridge, 2014).
[4] S. Surya, Living Rev. Relativ. **22**, 5 (2019) [arXiv:1903.11544 [gr-qc]] [Search INSPIRE].
[5] T. Konopka, F. Markopoulou, and L. Smolin, arXiv:hep-th/0611197 [Search INSPIRE].
[6] J. Ambjørn, B. Durhuus, and T. Jønsson, Mod. Phys. Lett. A **06**, 1133 (1991).
[7] N. Sasakura, Mod. Phys. Lett. A **06**, 2613 (1991).
[8] N. Godfrey and M. Gross, Phys. Rev. D **43**, R1749(R) (1991).
[9] R. Gurau, Commun. Math. Phys. **304**, 69 (2011) [arXiv:0907.2582 [hep-th]] [Search INSPIRE].
[10] P. Di Francesco, P. Ginsparg, and J. Zinn-Justin, Phys. Rep. **254**, 1 (1995) [arXiv:hep-th/9306153] [Search INSPIRE].

[9] A more rigorous way of defining the integral would be to express the integration contour as a sum of Lefschetz thimbles [33].

[11] V. Bonzom, R. Gurau, A. Riello, and V. Rivasseau, Nucl. Phys. B **853**, 174 (2011) [arXiv:1105.3122 [hep-th]] [Search INSPIRE].
[12] R. Gurau and J. P. Ryan, SIGMA **8**, 020 (2012) [arXiv:1109.4812 [hep-th]] [Search INSPIRE].
[13] J. Ambjørn, J. Jurkiewicz, and R. Loll, Phys. Rev. Lett. **93**, 131301 (2004) [arXiv:hep-th/0404156] [Search INSPIRE].
[14] N. Sasakura, Int. J. Mod. Phys. A **27**, 1250020 (2012) [arXiv:1111.2790 [hep-th]] [Search INSPIRE].
[15] N. Sasakura, Int. J. Mod. Phys. A **27**, 1250096 (2012) [arXiv:1203.0421 [hep-th]] [Search INSPIRE].
[16] N. Sasakura, Int. J. Mod. Phys. A **28**, 1350111 (2013) [arXiv:1305.6389 [hep-th]] [Search INSPIRE].
[17] G. Narain, N. Sasakura, and Y. Sato, J. High Energy Phys. **1501**, 010 (2015) [arXiv:1410.2683 [hep-th]] [Search INSPIRE].
[18] D. Obster and N. Sasakura, Eur. Phys. J. C **77**, 783 (2017) [arXiv:1704.02113 [hep-th]] [Search INSPIRE].
[19] D. Obster and N. Sasakura, Prog. Theor. Exp. Phys. **2018**, 043A01 (2018) [arXiv:1710.07449 [hep-th]] [Search INSPIRE].
[20] L. Lionni and N. Sasakura, Prog. Theor. Exp. Phys. **2019**, 073A01 (2019) [arXiv:1903.05944 [hep-th]] [Search INSPIRE].
[21] N. Sasakura and S. Takeuchi, Eur. Phys. J. C **80**, 118 (2020) [arXiv:1907.06137 [hep-th]] [Search INSPIRE].
[22] D. Obster and N. Sasakura, Prog. Theor. Exp. Phys. **2020**, 073B06 (2020) [arXiv:2004.03152 [hep-th]] [Search INSPIRE].
[23] N. Sasakura, PoS **CORFU2019**, 192 (2020) [arXiv:2004.07419 [hep-th]] [Search INSPIRE].
[24] L. Paniak and N. Weiss, J. Math. Phys. **36**, 2512 (1995) [arXiv:hep-th/9501037] [Search INSPIRE].
[25] V. A. Kazakov and P. Zinn-Justin, Nucl. Phys. B **546**, 647 (1999) [arXiv:hep-th/9808043] [Search INSPIRE].
[26] E. P. Wigner, Ann. Math. **62**, 548 (1955).
[27] E. Brézin, C. Itzykson, G. Parisi, and J. B. Zuber, Commun. Math. Phys. **59**, 35 (1978).
[28] J. Jurkiewicz, Phys. Lett. B **245**, 178 (1990).
[29] I. M. Gelfand, M. M. Kapranov, and A. V. Zelevinsky, *Discriminants, Resultants, and Multidimensional Determinants* (Birkhäuser, Boston, 1994).
[30] T. Castellani and A. Cavagna, J. Stat. Mech.: Theo. Exp. **P2005**, 05012 (2005) [arXiv:cond-mat/0505032 [cond-mat.dis-nn]].
[31] L. Qi, arXiv:1201.3424 [math.SP].
[32] N. Sasakura and Y. Sato, Phys. Lett. B **732**, 32 (2014) [arXiv:1401.2062 [hep-th]] [Search INSPIRE].
[33] E. Witten, AMS/IP Stud. Adv. Math. **50**, 347 (2011) [arXiv:1001.2933 [hep-th]] [Search INSPIRE].